The Astrophysical Journal Letters, 734:L8 (6pp), 2011 June 10 doi:10.1088/2041-8205/734/1/L8

THE VOLATILE COMPOSITION AND ACTIVITY OF COMET 103P/HARTLEY 2 DURING THE *EPOXI* CLOSEST APPROACH*

N. Dello Russo[1], R. J. Vervack, Jr.[1], C. M. Lisse[1], H. A. Weaver[1], H. Kawakita[2], H. Kobayashi[2], A. L. Cochran[3], W. M. Harris[4], A. J. McKay[5], N. Biver[6], D. Bockelée-Morvan[6], and J. Crovisier[6]
[1] Space Department, The Johns Hopkins University Applied Physics Laboratory, 11100 Johns Hopkins Rd., Laurel, MD 20723, USA; neil.dello.russo@jhuapl.edu
[2] Department of Physics, Faculty of Science, Kyoto Sangyo University Motoyama, Kamigamo, Kita-ku, Kyoto 603-8555, Japan
[3] McDonald Observatory, 1 University Station C1402, Austin, TX 78712–0259, USA
[4] Department of Applied Sciences, University of California-Davis, One Shields Avenue, Davis, CA 95616, USA
[5] Astronomy Department, New Mexico State University, Las Cruces, NM 88001, USA
[6] LESIA, Observatoire de Paris, 5 place Jules Janssen, 92195 Meudon, France
Received 2011 March 7; accepted 2011 March 25; published 2011 May 16

ABSTRACT

We report time-resolved measurements of the absolute and relative abundances of eight parent volatiles (H_2O, CH_3OH, C_2H_6, C_2H_2, NH_3, HCN, H_2CO, and HC_3N) in the coma of 103P/Hartley 2 on UT 2010 November 4, the date the *EPOXI* spacecraft made its closest approach to the comet, using high-dispersion infrared spectroscopy with NIRSPEC at the W. M. Keck Observatory. Overall gas and dust production increased by roughly 60% between UT 10:49 and 15:54. Differences in the spatial distributions of species in the coma suggest icy sources of different composition in the nucleus of 103P/Hartley 2. However, differences in the relative abundances of species with time are minor, suggesting either internal compositional heterogeneity in 103P/Hartley 2 is small compared with the diversity of chemistry observed within the comet population, or more significant heterogeneity exists on scales smaller than our spatial resolution. Observations contemporaneous with the *EPOXI* encounter test how compositional heterogeneity over the surface and the inner coma of a comet manifests itself in remote-sensing observations of the bulk coma.

Key words: astrochemistry – comets: general – comets: individual (103P/Hartley 2) – infrared: general – molecular data – techniques: spectroscopic

1. BACKGROUND

Consistent with their formation in the cold outer regions of the solar nebula, comet nuclei contain substantial amounts of ice (volatiles). As primitive objects, the volatile composition of comets is likely to provide key data on the formation and early evolution of the solar system. To explore the connections among the formation environment, subsequent chemical evolution, and present composition of comets, efforts have been made to develop a chemical taxonomy for comets (A'Hearn et al. 1995; Bockelée-Morvan et al. 2005; Feldman et al. 2005; Fink 2009). Jupiter-family comets are currently the most practical targets for spacecraft missions, so their comprehensive study is especially important in linking the global coma chemistry inferred from the growing remote-sensing database to compositional information on the spatially resolved nucleus and inner coma returned by in situ missions.

Comet 103P/Hartley 2 (hereafter Hartley 2) is a Jupiter-family comet of likely Kuiper Belt origin based on its short orbital period (6.5 years) and low orbital inclination (13°.6). The 2010 apparition provided the best observing conditions to date for Hartley 2 as it made an extremely close approach to Earth. As the target of the NASA *EPOXI* mission, Hartley 2 allowed for ground-based measurements of gas production, parent volatile inventory, and spatial distributions of volatiles in the coma to be directly compared to in situ spectroscopic and imaging results. We measured the volatile composition of Hartley 2 on multiple nights using the Near-Infrared Spectrometer (NIRSPEC) at the Keck II telescope on Mauna Kea, Hawaii (McLean et al. 1998). Data from UT 2010 November 4, covering the closest approach of the *EPOXI* spacecraft to the nucleus of Hartley 2, are described here.

2. OBSERVATIONS

Hartley 2 provided an excellent opportunity to search for chemical heterogeneity within a comet nucleus. Unlike the vast majority of comets, Hartley 2 appears to be active over most of its surface (Lamy et al. 2005; Tancredi et al. 2006; Lisse et al. 2009; A'Hearn et al. 2011), with discrete areas of diverse coma chemistry (A'Hearn et al. 2011). Radar observations, later confirmed by the *EPOXI* flyby, showed an elongated bilobate object (Harmon et al. 2011; A'Hearn et al. 2011) perhaps suggesting major components of different origins. Circumstances allowed the observation of Hartley 2 over a large fraction of its rotational period (Knight et al. 2010; Harmon et al. 2011) within a single night. Thus, we adopted an observing strategy to identify any variability of the absolute or relative production rates and/or the spatial distributions of volatiles with time.

For our observations of Hartley 2 we used a 24×0.432 arcsec slit (2700×50 km projected at the comet), resulting in a spectral resolving power ($\lambda/\Delta\lambda$) $\sim$ 28,000. NIRSPEC pixels subtend 0.144 arcsec and 0.190 arcsec in the spectral and spatial dimensions, respectively, resulting in a spatial resolution at the comet of $\sim$22 km pixel^{-1} on UT November 4. However, the practical spatial resolution is limited by the seeing which was $\sim$0.5 arcsec and relatively stable during the night.

Three grating settings were used during the night over five distinct time intervals (Table 1). For each setting, spectra were acquired using sequences of four scans with an integration time of one-minute on-source per scan (four minutes for the complete sequence). During a sequence of scans, the telescope

* Based on observations obtained at the W. M. Keck Observatory, Mauna Kea, HI, USA.

Table 1
Composition of Parent Volatiles in the Coma of 103P/Hartley 2 on UT 2010 November 4

Molecules Sampled	Lines Used	T_{rot} (K)	Production Rate (10^{25} s^{-1})	Relative Abundance
KL1A	**UT 10:49–11:30**	**24 minutes on-source**	**Slit P.A. = 284°**	
H_2O	18	66 ($^{+7}/_{-6}$)	884 ± 109	100
CH_3OH	21	75	12.6 ± 1.9	1.43 ± 0.19
C_2H_6	29	63 ($^{+8}/_{-7}$)	5.55 ± 0.69	0.63 ± 0.07
C_2H_2	3	70	1.37 ± 0.23	0.15 ± 0.02
NH_3	3	70	4.4 ± 1.1	0.50 ± 0.12
KL2	**UT 11:37–12:55**	**44 minutes on-source**	**Slit P.A. = 284°**	
H_2O	15	83 ($^{+10}/_{-6}$)	1120 ± 160	100
CH_3OH	9	75	12.6 ± 1.6	1.13 ± 0.15
C_2H_6	16	70 ($^{+7}/_{-6}$)	7.30 ± 0.98	0.65 ± 0.09
C_2H_2	10	78 ($^{+11}/_{-9}$)	1.55 ± 0.23	0.14 ± 0.02
NH_3	1	80	9.4 ± 1.9	0.84 ± 0.16
HCN	12	73 ± 3	3.06 ± 0.37	0.27 ± 0.03
H_2CO	1	80	1.27 ± 0.23	0.11 ± 0.02
KL3	**UT 13:33–14:43**	**40 minutes on-source**	**Slit P.A. = 284°**	
H_2O	30	84 ($^{+5}/_{-4}$)	1270 ± 160	100
CH_3OH	14	75	16.2 ± 2.1	1.28 ± 0.14
C_2H_6	5	80	10.2 ± 1.5	0.80 ± 0.11
C_2H_2	9	92 ($^{+21}/_{-14}$)	1.64 ± 0.31	0.13 ± 0.02
NH_3	4	80	7.4 ± 2.1	0.58 ± 0.16
HCN	11	84 ($^{+14}/_{-11}$)	3.10 ± 0.39	0.24 ± 0.03
H_2CO	1	80	1.41 ± 0.27	0.11 ± 0.02
HC_3N	19	80	<0.31	<0.024
KL1B	**UT 14:50–15:17**	**16 minutes on-source**	**Slit P.A. = 284°**	
H_2O	18	73 ($^{+7}/_{-6}$)	1400 ± 170	100
CH_3OH	21	75	16.9 ± 2.0	1.21 ± 0.12
C_2H_6	29	68 ($^{+9}/_{-8}$)	10.1 ± 1.2	0.72 ± 0.07
C_2H_2	3	70	1.93 ± 0.36	0.14 ± 0.02
NH_3	3	70	7.3 ± 2.3	0.52 ± 0.16
KL1C	**UT 15:20–15:54**	**20 minutes on-source**	**Slit P.A. = 5°**	
H_2O	18	69 ($^{+6}/_{-5}$)	1380 ± 160	100
CH_3OH	21	75	16.8 ± 2.0	1.22 ± 0.12
C_2H_6	29	63 ± 7	12.7 ± 1.5	0.92 ± 0.08
C_2H_2	3	70	2.21 ± 0.70	0.16 ± 0.05
NH_3	3	70	8.1 ± 1.9	0.59 ± 0.14

Notes. The setting name, time interval, time on-source, and slit position angle are given. The heliocentric distance, geocentric distance, and geocentric velocity were 1.064 AU, 0.156 AU, and +7 km s^{-1}, respectively. The time of the *EPOXI* closest approach was UT 14:02 as observed from Earth. The total number of emission lines used to determine production rates and rotational temperatures for each species are given. Assumed rotational temperatures are values listed without uncertainties.

was nodded 12 arcsec between A and B positions in an ABBA pattern keeping the comet on-slit for all integrations.

3. DATA ANALYSIS

An extensive description of the data processing techniques is given elsewhere (Bonev 2005; Dello Russo et al. 2006); only the most relevant details are discussed here. Spectral frames were registered such that the spectral and spatial dimensions fell along rows and columns, respectively. Spectra were then extracted over the desired spatial extent and position along the slit (Figure 1). Atmospheric models were obtained using the FASCOD3 transmittance model, an updated version of the original FASCOD model (Clough et al. 1981, 1988) accessing the HITRAN-2004 Molecular Database (Rothman et al. 2005). Atmospheric models were used to assign wavelength scales to the extracted spectra and to establish absolute column abundances for each important absorbing species in the terrestrial atmosphere. The synthetic transmittance model is scaled to continuum points in regions of the comet spectrum that have high atmospheric transmittance and are also free of any apparent cometary molecular emissions.

The molecular emissions are isolated from the dust emission by subtracting a modeled dust continuum from the comet spectrum row by row, yielding the net cometary molecular emission intensities along the slit (still convolved with the atmospheric transmittance function). The true line flux incident at the top of the terrestrial atmosphere was determined within a given aperture by dividing the observed flux by the monochromatic transmittance at the Doppler-shifted line position.

Production rates, rotational temperatures, and ortho-to-para ratios (OPRs) were derived from the column densities within nucleus-centered extracts by applying a coma model assuming spherically symmetric outflow with uniform velocity. Although asymmetries will likely have a small residual effect on our global production rates, this method has been shown to be a valid approach to first order (Xie & Mumma 1996). Production rates derived from nucleus-centered extracts are always low owing to slit losses, so a correction (referred to as the "multiplicative growth factor") was applied using regions offset from the nucleus where the model is less affected by slit losses. We

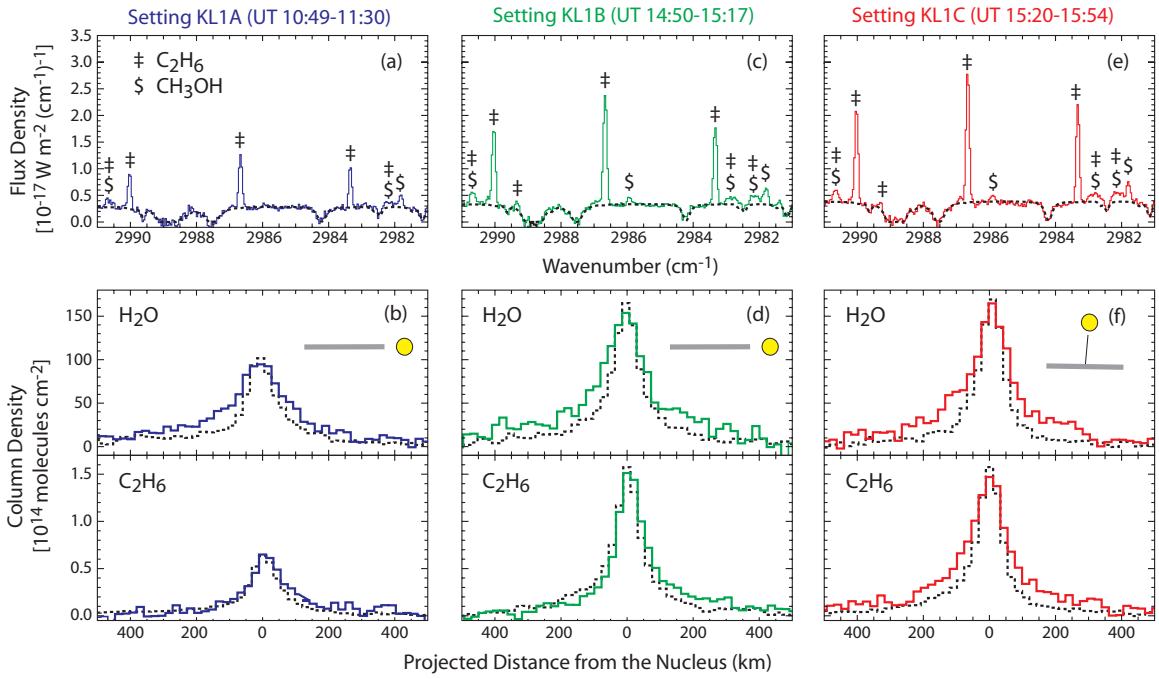

Figure 1. Spectra and spatial distributions of volatiles and dust in 103P/Hartley 2 on UT 2010 November 4. The three sets of panels correspond to data obtained during three of the five time intervals. (a) A flux-calibrated spectrum illustrating the detection of C_2H_6 and CH_3OH during the indicated time interval. The spectrum is coadded over 3 spectral × 9 spatial pixels (0.43 × 1.74 arcsec) centered on the peak of the dust continuum. Solid colored traces are the comet spectra with best-fit atmospheric models superimposed (dashed black traces). The 1σ noise level is $\sim 1.5 \times 10^{-19}$ W m^{-2} (cm^{-1})$^{-1}$. (b) Spatial distributions of C_2H_6 (lower half) and H_2O (upper half) along the slit during the same time interval as (a). The solid colored traces refer to the volatile species; the dashed traces refer to the dust. Noise levels (1σ) are $\sim 0.03 \times 10^{16}$ molec cm^{-2} for C_2H_6 and $\sim 4 \times 10^{16}$ molec cm^{-2} for H_2O. The slit orientation with respect to the Sun is shown. (c)–(d) and (e)–(f) are similar to (a)–(b) but for the two additional time intervals as indicated.

assumed a gas outflow velocity of $v = (800 \times R_h^{-0.5}) = 776$ m s^{-1}, where R_h is the heliocentric distance in AU. The transit time for molecules from the nucleus to the edge of the field of view (in the plane of the sky) is short compared to the lifetime of all measured species so the derived production rates are proportional to the assumed outflow velocity.

Fluorescence models have been developed for all sampled parent volatiles in order to convert spectral line fluxes into gas rotational temperatures and production rates and have been used to determine fluorescence efficiencies (g-factors) for relevant molecules over a range of temperatures typically found in the inner comae of comets (e.g., 10–200 K). The development of fluorescence models for linear molecules such as CO, HCN, HC_3N, and C_2H_2 is straightforward, whereas fluorescence models for H_2O, C_2H_6, and H_2CO are more complicated (Reuter et al. 1989; Dello Russo et al. 2001, 2004; DiSanti et al. 2006). An NH_3 fluorescence model was developed based on band strengths (Kleiner et al. 1999), equations for transition intensities, Hönl–London factors and Herman–Wallis-type corrections for the NH_3 ν_1 band (Pine & Dang-Nhu 1993), and Einstein A-coefficients for individual rotational–vibrational transitions from the HITRAN database (Rothman et al. 2005). CH_3OH production rates were derived from analysis of the ν_3 Q-branch when available. We used a g-factor for the ν_3 Q-branch of 2.17×10^{-5} s^{-1} at 1 AU (Bockelée-Morvan et al. 1995). To increase the time interval over which CH_3OH production rates could be determined, additional CH_3OH lines were used in the analysis by comparing CH_3OH line intensities in Hartley 2 to those seen in survey spectra for comet C/1999 H1 Lee (Dello Russo et al. 2006). The gas rotational temperatures derived in C/1999 H1 Lee for CO, C_2H_6, HCN, and H_2O on UT 1999 August 21.6 were between 65 and 80 K (Mumma et al. 2001; Dello Russo et al. 2006), similar to gas rotational temperatures derived for Hartley 2 (Table 1). Therefore, assuming the relative intensities of detected CH_3OH lines and the ν_3 Q-branch are the same in both comets, g-factors were determined empirically for CH_3OH lines detected in other settings. The scatter in production rates determined for individual CH_3OH lines using this method is similar in magnitude to that seen in other species where fluorescence models were used.

4. RESULTS AND DISCUSSION

4.1. Rotational Temperatures and Water Ortho-to-Para Ratio

In cases where the measurement of multiple lines with a range of ground-state rotational energies was possible, rotational temperatures were determined from a Boltzmann analysis of the relative intensities of individual lines (Dello Russo et al. 2004). Measured gas rotational temperatures ranged from 63 to 92 K and did not show any clear evidence of variability with time or differences among species (Table 1).

Multiple ortho and para H_2O lines in each grating setting was used to determine H_2O OPRs and nuclear spin temperatures. The importance of OPRs is disputed, but they may preserve information about conditions in comet-forming regions in the early solar nebula (Mumma et al. 1993). The technique used for deriving OPRs and their associated uncertainties is described elsewhere (Dello Russo et al. 2005). For Hartley 2, OPRs and nuclear spin temperatures were determined independently in each grating setting. The weighted average from all settings gives OPR = 3.4 ± 0.6 and $T_{spin} \geqslant 38$ K (95% confidence

intervals). This lower limit is marginally higher than a previous measurement on Hartley 2 of 34 ± 3 K with the *Infrared Space Observatory* (Crovisier et al. 1999).

4.2 Production Rates and Relative Abundances

Absolute and relative production rates in Hartley 2 on UT November 4 are given in Table 1. Production rates listed for each species are determined from a weighted average of production rates derived independently for all detected lines (the number of lines used in the analysis is given in Table 1). In the case of HC_3N, where an upper limit is reported, a production rate was calculated independently over each HC_3N line position for which there were no known blends and the atmospheric transmittance was at least 85%. The production rate derived from a weighted average of 19 lines gave a 2.7σ positive residual ($Q = (1.9 \pm 0.7) \times 10^{24}$ s^{-1}; $HC_3N/H_2O = (1.5 \pm 0.6) \times 10^{-4}$). This marginal signal is reported as an upper limit at the 95% confidence interval in Table 1. This is the first reported HC_3N production rate in a comet from infrared wavelengths, and its abundance relative to HCN is consistent with what is typically measured at radio wavelengths (Bockelée-Morvan et al. 2005).

Uncertainties in individual line fluxes include photon noise (reflecting the signal-to-noise ratios in these lines). However, uncertainties in the derived rotational temperatures, OPRs, and absolute production rates are not dominated by the signal-to-noise ratios of individual spectral lines, which are generally high (Figure 1), but by line-by-line deviations between the best-fit fluorescence model and the data. Thus, reported uncertainties reflect the standard deviation from the mean of individual line measurements and the effects of small-number statistics. In addition, uncertainties for the nucleus-to-terminal correction factors or growth factors (measured to be between ∼3% and 10% depending on the species and setting), flux calibration (estimated at 10%) and rotational temperature (estimated ± 10 K uncertainty for assumed values of T_{rot}) were also included in absolute production rate error bars. Uncertainties for relative production rates in Table 1 do not include uncertainty in flux calibration because all lines and species were detected within the same grating setting.

4.3. Variable Activity and Heterogeneity of Volatiles in the Coma of 103P/Hartley 2

Significant short-term variability in comet activity was measured with the overall gas and dust production increasing by ∼60% over the course of the night (Table 1; Figures 1 and 2). Within uncertainties this increase in total gas production rate was uniform among all measured species with the possible exception of C_2H_6, which appeared to increase more rapidly than other species during the night (Figure 2). This differential increase in C_2H_6 was most pronounced between time intervals four and five (Table 1; Figures 1 and 2), suggesting that a change in slit orientation likely contributed to this measured increase.

Whereas the temporal evolution of relative volatile abundances provided only a tenuous indication of chemical heterogeneity within Hartley 2, the spatial distribution of volatiles in the coma provides more compelling evidence. In each grating setting, an integrated column density along the slit was obtained by summing multiple lines for each species. During the first four time intervals, when the slit was oriented along the extended heliocentric radius vector (position angle, P.A. = 284°), H_2O and CH_3OH have spatial distributions similar to each other that show evidence for slightly extended source regions relative

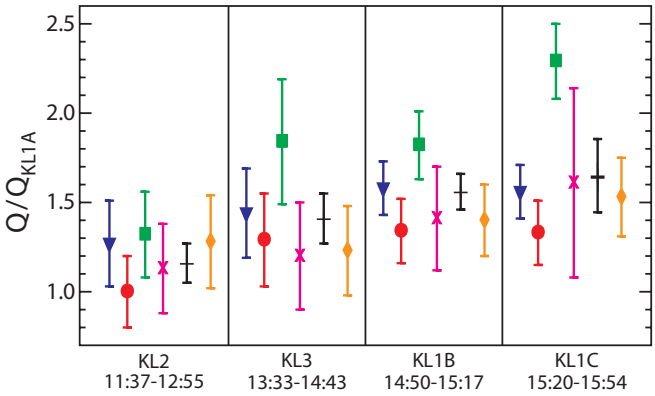

Figure 2. Temporal variability of volatile and dust production in 103P/Hartley 2 on UT 2010 November 4. Ratios of the production rates for species in four settings relative to initial observations in setting KL1A (UT 10:49–11:30) are shown. The setting names and range of UT times for observations are given below the *x*-axis. The slit position angle was 5° in setting KL1C and 284° for all other settings (see Table 1). Species include H_2O (blue triangles), CH_3OH (red circles), C_2H_6 (green squares), C_2H_2 (pink × s), and dust at 2.9 mm (gold diamonds). The weighted average of the four volatile species is also shown (black +s).

to the dust (Figures 1 and 3). This is different from the distribution of C_2H_6, which shows no similar extension relative to the dust in the antisunward direction (Figures 1 and 3). When the slit position angle was changed to 5° during time interval five, the spatial distribution of C_2H_6 appeared more extended—similar to H_2O and CH_3OH (Table 1; Figure 1). This increased spatial extent of C_2H_6 along the slit in the last time interval is consistent with a jump in its measured production rate during this time (Table 1; Figure 2).

Spatial distributions for HCN and C_2H_2 were also obtained in settings KL2 and KL3 (Table 1; Figure 3). Their spatial distributions appear similar to each other and to C_2H_6 (Figure 3). This suggests that sources for HCN and C_2H_2 may be more closely associated with C_2H_6 than with H_2O or CH_3OH, but this link is tenuous as we lack information about how the spatial distribution of HCN and C_2H_2 change with slit orientation. Based on encounter images from *EPOXI* revealing large grains in the vicinity of the nucleus (A'Hearn et al. 2011), the differences in spatial profiles may be at least partially explained by more extended release of H_2O- and CH_3OH-rich icy grains in the antisunward direction.

4.4. The Chemical Relationship of 103P/Hartley 2 to Other Comets

When comparing relative production rates of volatile species with other comets, we find the following approximate relationships in Hartley 2: C_2H_6/H_2O (typical); HCN/H_2O (typical); C_2H_2/H_2O (typical); CH_3OH/H_2O (typical); NH_3/H_2O (typical); H_2CO/H_2O (depleted). *Hubble Space Telescope* observations on the night of encounter and previous infrared measurements of Hartley 2 with NIRSPEC suggest that hypervolatiles CH_4 and CO are also depleted with respect to H_2O (Dello Russo et al. 2010; Weaver et al. 2011). Knowledge of the volatile chemistry of Jupiter-family comets from infrared observations is limited, with the few Jupiter-family comets sampled to date showing diverse compositions (Figure 4; Mumma et al. 2005; Dello Russo et al. 2007, 2008, 2009). This diversity is notable given the similarity in composition between fragments of 73P/Schwassmann-Wachmann 3 (Figure 4; Dello Russo et al. 2007), another comet with high surface activity studied during

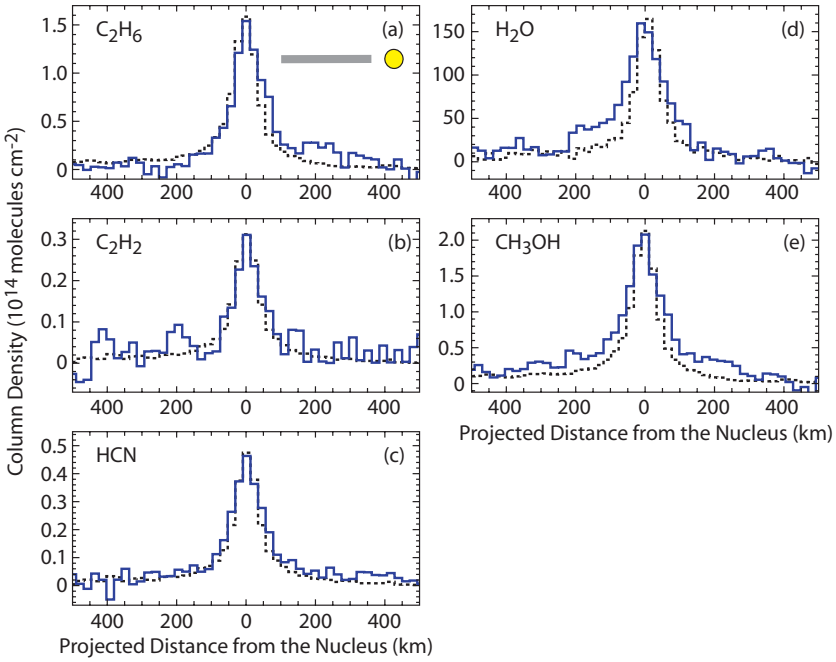

Figure 3. Spatial distributions of volatiles (solid blue traces) and dust (dashed traces) in 103P/Hartley 2 on UT 2010 November 4. Spatial profiles are from setting KL3, taken nearest in time to the *EPOXI* closest approach. (a)–(c) The spatial distributions of (a) C_2H_6, (b) C_2H_2, and (c) HCN appear similar to each other and to the dust. Spatial distributions for (d) H_2O and (e) CH_3OH are similar to each other but appear more extended, especially in the antisunward direction, compared with C_2H_6, C_2H_2, and HCN. The slit orientation with respect to the Sun for all panels is shown in (a).

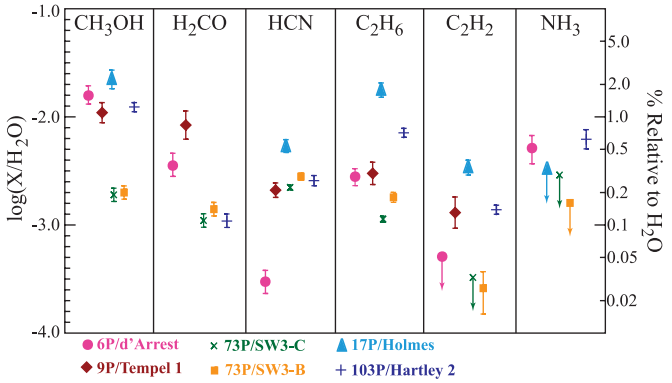

Figure 4. Compositional comparison of Jupiter-family comets. Abundances relative to H_2O are given for six species from ground-based infrared spectroscopy (Dello Russo et al. 2007, 2008, 2009; Mumma et al. 2005). Symbols with downward arrows denote 3σ upper limits.

its very close approach to Earth in 2006. Although Hartley 2 and Schwassmann-Wachmann 3 have significantly different chemical compositions, the evidence from ground-based observations supports only small-scale chemical heterogeneity for both comets despite significant short-term variability in activity, and in the case of Schwassmann-Wachmann 3, between measurements of different fragments.

4.5. Synergy with EPOXI Encounter Data

The spectral and spatial information obtained from this study are highly complementary to the *EPOXI* spectroscopic and imaging data obtained near closest approach. The *EPOXI* HRI-IR spectrometer can detect general emission features due to organics; however, it is unable to resolve emissions from specific organic species. The high spectral resolution of the NIRSPEC observations allows the detection, isolation and quantification of gas production rates from highly diagnostic rotational–vibrational lines. This information can be used to help interpret unresolved features in HRI-IR spectra.

A general organic X-CH feature has been seen between 3.3 and 3.6 μm in low-resolution spectra of comets, resulting from emission due to gas-phase organics, primarily CH_3OH and C_2H_6 (Bockelée-Morvan et al. 1995; Dello Russo et al. 2006). Additional volatile species can also contribute flux to the X-CH feature, but based on high-resolution infrared spectra of previous comets, contributions from other species are generally minor (probably $\leqslant$10% in most cases). Based on the band g-factors and mixing ratios of these species derived from NIRSPEC observations, the relative contribution of C_2H_6 and CH_3OH band intensities to the total flux of the X-CH feature is $(C_2H_6)/(CH_3OH) \sim 0.8$ for Hartley 2 on UT 2010 November 4.

HRI-IR is able to detect and isolate strong emissions from H_2O and CO_2 fundamental bands; however, optical depth effects complicate their interpretation (A'Hearn et al. 2005). This problem is compounded around encounter because the overall gas production rates and opacity were varying substantially at a time when the spacecraft viewing geometry was changing rapidly. Thus, information on the short-term variability of the gas production rates as determined here will facilitate the interpretation of HRI-IR spectra near closest approach. Our wide spatial view of the distribution of gases in the coma also complements the contemporaneous and extremely high spatial resolution information retrieved by *EPOXI*, which was obtained at the price of a limited field of view near closest approach.

Long-term monitoring of parent volatile production rates in individual comets has revealed variable coma compositions in some comets (e.g., Biver et al. 2002). However, as molecular sublimation rates are dependent on temperature (and heliocentric distance), there is little convincing evidence from remote-sensing observations for significant chemical

heterogeneity for ices within individual comet nuclei. This may suggest that the building blocks that constitute an individual comet are less heterogeneous than the population as a whole. However, apart from exceptional circumstances, remote-sensing techniques sample the bulk coma over spatial resolutions that tend to homogenize the composition and therefore are ill equipped to determine the full extent of chemical diversity within a comet. The close approach of 73P/Schwassmann-Wachmann 3 to Earth and the ability to chemically sample individual fragments provided a unique opportunity (Dello Russo et al. 2007), but accompanying spacecraft observations at close range do not exist. Ground-based observations contemporaneous with the *EPOXI* closest approach to Hartley 2 provide the best test to date of how compositional heterogeneity over the surface and the inner coma of a comet manifests itself in remote-sensing observations of the bulk coma.

The NASA PAST and PATM Programs support this work. Data were obtained at the W. M. Keck Observatory. The observatory was made possible by the financial support of the W. M. Keck Foundation. We thank Julie Renaud-Kim and Al Conrad for their assistance and expertise. We acknowledge the significant cultural role that Mauna Kea has always had within the indigenous Hawaiian community, and are grateful to have the opportunity to conduct these observations.

REFERENCES

A'Hearn, M. F., Millis, R. L., Schleicher, D. G., Osip, D. J., & Birch, P. V. 1995, Icarus, 118, 223
A'Hearn, M. F., et al. 2005, Science, 310, 258
A'Hearn, M. F., et al. 2011, Science, in press
Biver, N., et al. 2002, Earth Moon Planets, 90, 5
Bockelée-Morvan, D., Brooke, T. Y., & Crovisier, J. 1995, Icarus, 116, 18
Bockelée-Morvan, D., Crovisier, J., Mumma, M. J., & Weaver, H. A. 2005, in Comets II, ed. M. C. Festou, H. U. Keller, & H. A. Weaver (Tucson, AZ: Univ. Arizona Press), 391
Bonev, B. P. 2005, in PhD thesis, Univ. Toledo
Clough, S. A., Kneizys, F. X., Rothman, L. S., & Gallery, W. O. 1981, Proc. SPIE, 277, 152
Clough, S. A., et al. 1988, in IRS'88: Current Problems in Atmospheric Radiation, ed. J. Lenoble (Hampton, VA: A. Deepak), 372
Crovisier, J., et al. 1999, The Universe as seen by *ISO* (ESA SP-427; Noordwijk: ESA), 161
Dello Russo, N., Bonev, B. P., DiSanti, M. A., Mumma, M. J., Gibb, E. L., Magee-Sauer, K., Barber, R. J., & Tennyson, J. 2005, ApJ, 621, 537
Dello Russo, N., DiSanti, M. J., Magee-Sauer, K., Gibb, E. L., M. A., Mumma, Barber, R. J., & Tennyson, J. 2004, Icarus, 168, 186
Dello Russo, N., Mumma, M. J., DiSanti, M. A., Magee-Sauer, K., Gibb, E. L., Bonev, B. P., McLean, I. S., & Xu, L-H. 2006, Icarus, 184, 255
Dello Russo, N., Mumma, M. J., DiSanti, M. J., Magee-Sauer, K., & Novak, R. 2001, Icarus, 153, 162
Dello Russo, N., Vervack, R. J., Jr., Kawakita, H., & Kobayashi, H. 2010, IAU Circ., 9171, 1
Dello Russo, N., Vervack, R. J., Jr., Weaver, H. A., Biver, N., Bockelée-Morvan, D., Crovisier, J., & Lisse, C. M. 2007, Nature, 448, 172
Dello Russo, N., Vervack, R. J., Weaver, H. A., Kawakita, H., Kobayashi, H., Biver, N., Bockelée-Morvan, D., & Crovisier, J. 2009, ApJ, 703, 187
Dello Russo, N., Vervack, R. J., Jr., Weaver, H. A., Montgomery, M. M., Deshpande, R., Fernández, Y. R., & Martin, E. L. 2008, ApJ, 680, 793
DiSanti, M. A., Bonev, B. P., Magee-Sauer, K., Dello Russo, N., Mumma, M. J., Reuter, D., & Villanueva, G. L. 2006, ApJ, 650, 470
Feldman, P., Cochran, A. L., & Combi, M. R. 2005, in Comets II, ed. M. C. Festou, H. U. Keller, & H. A. Weaver (Tucson, AZ: Univ. Arizona Press), 425
Fink, U. 2009, Icarus, 201, 311
Harmon, J. K., Nolan, M. C., Howell, E. S., Giorgini, J. D., & Taylor, P. A. 2011, ApJ, 734, L2
Kleiner, I., Brown, L. R., Tarrago, G., Kou, Q-L., Picqué, N., Guelachvili, G., Dana, V., & Mandin, J-Y. 1999, J. Mol. Spectrosc., 193, 46
Knight, M., Schwieterman, E., & Schleicher, D. 2010, IAU Circ., 9163, 2
Lamy, P., Toth, I., Fernández, Y. R., & Weaver, H. A. 2005, in Comets II, ed. M. C. Festou, H. U. Keller, & H. A. Weaver (Tucson, AZ: Univ. Arizona Press), 223
Lisse, C. M., et al. 2009, PASP, 121, 968
McLean, I. A., et al. 1998, Proc. SPIE, 3354, 566
Mumma, M. J., Weissman, P. R., & Stern, S. A. 1993, in Protostars and Planets III, ed. E. H. Levy & J. I. Lunine (Tucson, AZ: Univ. Arizona Press), 1177
Mumma, M. J., et al. 2001, ApJ, 546, 1183
Mumma, M. J., et al. 2005, Science, 310, 270
Pine, A. S., & Dang-Nhu, M. 1993, J. Quant. Spectrosc. Radiat. Transfer, 50, 565
Reuter, D. C., Mumma, M. J., & Nadler, S. 1989, ApJ, 341, 1045
Rothman, L. S., et al. 2005, J. Quant. Spectrosc. Radiat. Transfer, 96, 139
Tancredi, G., Fernández, J. A., Rickman, H., & Licandro, J. 2006, Icarus, 182, 527
Weaver, H. A., Feldman, P. D., A'Hearn, M. F., Dello Russo, N., & Stern, S. A. 2011, ApJ, 734, L5
Xie, X., & Mumma, M. J. 1996, ApJ, 464, 457